Petersen ET, Lim T, Golay XModel-free arterial spin labeling quantification approach for perfusion MRI. Magn Reson Med 55:219-232

3 AUTHORS:

Esben Thade Petersen
University Medical Center Utrecht
62 PUBLICATIONS **964** CITATIONS

SEE PROFILE

Tchoyoson C C Lim
National Neuroscience Institute
134 PUBLICATIONS **1,579** CITATIONS

SEE PROFILE

Xavier Golay
University College London
164 PUBLICATIONS **4,922** CITATIONS

SEE PROFILE

Model-Free Arterial Spin Labeling Quantification Approach for Perfusion MRI

Esben Thade Petersen,[1,2] Tchoyoson Lim,[1] and Xavier Golay[1,3*]

In this work a model-free arterial spin labeling (ASL) quantification approach for measuring cerebral blood flow (CBF) and arterial blood volume (aBV) is proposed. The method is based on the acquisition of a train of multiple images following the labeling scheme. Perfusion is obtained using deconvolution in a manner similar to that of dynamic susceptibility contrast (DSC) MRI. Local arterial input functions (AIFs) can be estimated by subtracting two perfusion-weighted images acquired with and without crusher gradients, respectively. Furthermore, by knowing the duration of the bolus of tagged arterial blood, one can estimate the aBV on a voxel-by-voxel basis. The maximum of the residue function obtained from the deconvolution of the tissue curve by the AIF is a measure of CBF after scaling by the locally estimated aBV. This method provides averaged gray matter (GM) perfusion values of 38 ± 2 ml/min/100 g and aBV of 0.93% ± 0.06%. The average CBF value is 10% smaller than that obtained on the same data set using the standard general kinetic model (42 ± 2 ml/min/100 g). Monte Carlo simulations were performed to compare this new methodology with parametric fitting by the conventional model.   Magn Reson Med 55: 219–232, 2006. © 2006 Wiley-Liss, Inc.

Key words: arterial spin labeling; deconvolution; cerebral blood flow; arterial blood volume; regional perfusion imaging; 3.0 Tesla

Perfusion is a very important parameter that provides pathophysiological information about the condition of an organ. For instance, an accurate perfusion measurement can demonstrate whether an ischemic organ is viable or not. Another example is cancer, in which increased perfusion may be related to the aggressiveness (grade) of the tumor. Currently, several methods based on magnetic resonance imaging (MRI), computed tomography (CT), or nuclear medicine imaging are capable of measuring perfusion in different parts of the body.

[1]Department of Neuroradiology, National Neuroscience Institute, Singapore.

[2]Department of Biomedical Engineering, Nanyang Technological University, Singapore.

[3]Department of Electrical and Electronic Engineering, Nanyang Technological University, Singapore.

*Correspondence to: Xavier Golay, Ph.D., Department of Neuroradiology, National Neuroscience Institute, 11 Jalan Tan Tock Seng, Singapore 308433. E-mail: Xavier_Golay@nni.com.sg

Among MRI methods, arterial spin labeling (ASL) techniques have in recent years shown their potential for tissue perfusion quantification (1). The complete noninvasiveness and nonionizing nature of the technique makes ASL a very interesting method for studying perfusion in healthy individuals or patients who require repetitive follow-ups. With conventional radiological methods, such patients could be exposed to an elevated risk of developing cancer. Furthermore, the use of any radioactive tracers or exogenous contrast agents, which are necessary in most conventional techniques, may be restricted in patients with particular conditions, such as kidney failure, or in pediatric populations. Finally, ASL-based methods are useful for functional studies (2) and evaluations of new medications, in which physiological changes due to the pharmacological stimuli must be monitored over time (3).

The common goal of all existing ASL techniques is to produce a flow-sensitized image (also known as a labeled image) and a control image in which the static tissue signals are identical. This is usually performed by inverting or saturating the water protons in the blood supplying the imaged region. After a delay between labeling and image acquisition, called the inversion delay (TI), the labeled blood spins reach the capillaries, where they exchange with tissue water, giving rise to the perfusion signal. The subtraction of the label from the control yields a difference signal that directly reflects local perfusion, since the signal from stationary tissue is completely eliminated.

Quantitative CBF estimation is traditionally carried out using the tracer clearance theory originally proposed by Kety and Schmidt (4), and was first adapted to ASL experiments by Williams et al. (5). This original model assumed that the inverted arterial blood water is a freely diffusible tracer, and therefore implied that the exchange of this tracer with tissue water is instantaneous upon its arrival to the parenchyma. The resulting model therefore described tracer kinetics using a single compartment. Further assumptions were made, such as the use of a nondispersed square input function or negligible transit time of the tracer. However, while the validity of such assumptions is reasonable in healthy individuals, it becomes questionable in pathological cases, and may result in biased estimation of CBF. Buxton et al. (6) developed a general kinetic model to describe the magnetization difference between the control and label experiments in ASL, which included effects such as transit time.

Here we propose a model-free ASL quantification approach based on a deconvolution technique. Since the method does not include any modeling of an exchange

mechanism, its usefulness is relatively universal throughout the whole body. In the present study, brain perfusion will be demonstrated. To calculate perfusion, the exact temporal length of the bolus of tagged arterial blood, and a precise acquisition of the arterial input function (AIF) and the tissue curve at a high temporal resolution are required. For this reason, a new pulse sequence was developed that is capable of acquiring data at multiple time points while providing a well defined bolus. This new sequence was dubbed quantitative STAR labeling of arterial regions (QUASAR) and uses the labeling module of the recently published pulsed STAR labeling of arterial regions (PULSAR) sequence (7). Both techniques are capable of performing oblique labeling, which allows imaging of individual perfusion territories (8). The combined method was evaluated for cerebral blood flow (CBF) measurement in 13 healthy volunteers, and compared with the modified standard general kinetic model (6,9).

THEORY

Perfusion Quantification

Perfusion imaging using ASL encompasses both physiological mass transport and exchange mechanisms, which are most often considered as linear stationary systems for which superposition is applicable. In general, the linearity of a system can be assessed if its inputs and outputs are additive, and its homogeneity is guaranteed if they can be multiplied by a scalar. Stationarity implies time-invariance of the system's response to shifts in its given input. These are reasonable assumptions in an ASL perfusion experiment that lasts several minutes, during which time no major physiological alterations are expected.

Assuming both time-invariance and mass conservation, various methods for flow quantification have been proposed (4). Among others, Meier and Zierler (10) employed time-domain impulse functions to describe and compute perfusion using convolution. This idea was used by Gobbel and Fike (11) and Ostergaard et al. (12) for model-independent perfusion estimation by means of contrast bolus tracking using CT and MRI, respectively. Using this theory, the tissue perfusion F_t is calculated using the deconvolution of the tissue curve $C(t)$ by the measured arterial input function $C_a(t)$:

$$C(t) = F_t C_a(t) \otimes R(t) = F_t \int_0^t C_a(\tau) R(t - \tau) d\tau \quad [1]$$

$R(t)$ is the residue function that describes the fraction of contrast that remains in the system after a given time t. From the resulting product $F_t \cdot R(t)$, F_t can be separated because $R(0) = 1$.

For pulsed ASL (PASL), single-compartment Kety models (13–15) as well as more elaborate multicompartmental approaches have been proposed (16,17). Buxton et al. (6) described a general kinetic model for the magnetization difference between labeled and control measurements using the convolution integral:

$$\Delta M(t) = 2 \cdot M_{a,0} \cdot f \cdot \int_0^t c(\tau) \cdot r(t - \tau) \cdot m(t - \tau) d\tau \quad [2]$$

where $M_{o,a}$ is the equilibrium magnetization in a blood-filled voxel, f is the perfusion value, $c(t)$ is the delivery function or fractional arterial input function (AIF), and $r(t\text{-}\tau)$ is the residue function that describes the fraction of labeled spins arriving at a voxel at time τ that still remains within the voxel at time t. The magnetization relaxation term $m(t\text{-}\tau)$ quantifies the longitudinal magnetization fraction of labeled spins arriving at the voxel at time τ that remains at time t.

The commonly used standard model for PASL is based on the assumption of a uniform plug flow, and considering relaxation, the delivery function can be expressed as

$$c(t) = \begin{cases} 0, & t < \tau_a \\ e^{-t R_{l a}}, & \tau_a \leq t < \tau_d \\ 0, & t \geq \tau_d \end{cases} \quad [3]$$

where τ_a = arterial transit time, τ_d = time for the trailing edge of the labeled blood bolus to reach the tissue, and R_{1a} = longitudinal relaxation rate of arterial blood.

Applying single-compartment kinetics, or instantaneous mixing between arterial blood and tissue, Eq. [2] becomes

$$\Delta M(t) =$$

$$\begin{cases} 0, & t < \tau_a \\ \dfrac{-2 \cdot M_{a,0} \cdot f}{\delta R} e^{-R_{lo} t}(1 - e^{-\delta R(t - \tau_a)}), & \tau_a \leq t < \tau_d \\ \dfrac{-2 \cdot M_{a,0} \cdot f}{\delta R} e^{-R_{lo} \tau_d}(1 - r^{-\delta R(1 - \tau_a)}) \cdot e^{-R_{lapp}(t - \tau_d)}, & t \geq \tau_d \end{cases}$$

$$[4]$$

where $\delta R = R_{1a} - R_{1app}$ and $R_{1app} = R_1 + f/\lambda$, also called the apparent tissue relaxation rate, and λ is the blood-tissue partition coefficient.

From Eq. [4] it can be seen that various parameters, such as the transit time τ_a and blood-tissue partition coefficient λ, must be estimated or measured in order to obtain quantitative CBF values. Traditionally, PASL has been performed at a single inversion time point without information about transit time, which can lead to serious errors in the estimation of perfusion. To render ASL less sensitive to transit time, sequences such as QUIPSS II and Q2-TIPS (18,19) were developed. The principle of these techniques is to saturate the part of the label that remains within the labeling slab at a time delay that is short enough for the trailing edge of the fastest blood to remain within the inversion slab. However, if the distribution of transit times is wide (e.g., as in patients with atherosclerosis), these methods will fail. This problem can be solved by acquiring images at multiple inversion times and thereby measuring the entire ΔM curve. This lengthy process may not be applicable for clinical examinations, since typically 30−40 pairs of subtracted control and labeled images are required to obtain the desired signal-to-noise ratio (SNR) in the perfusion-weighted maps.
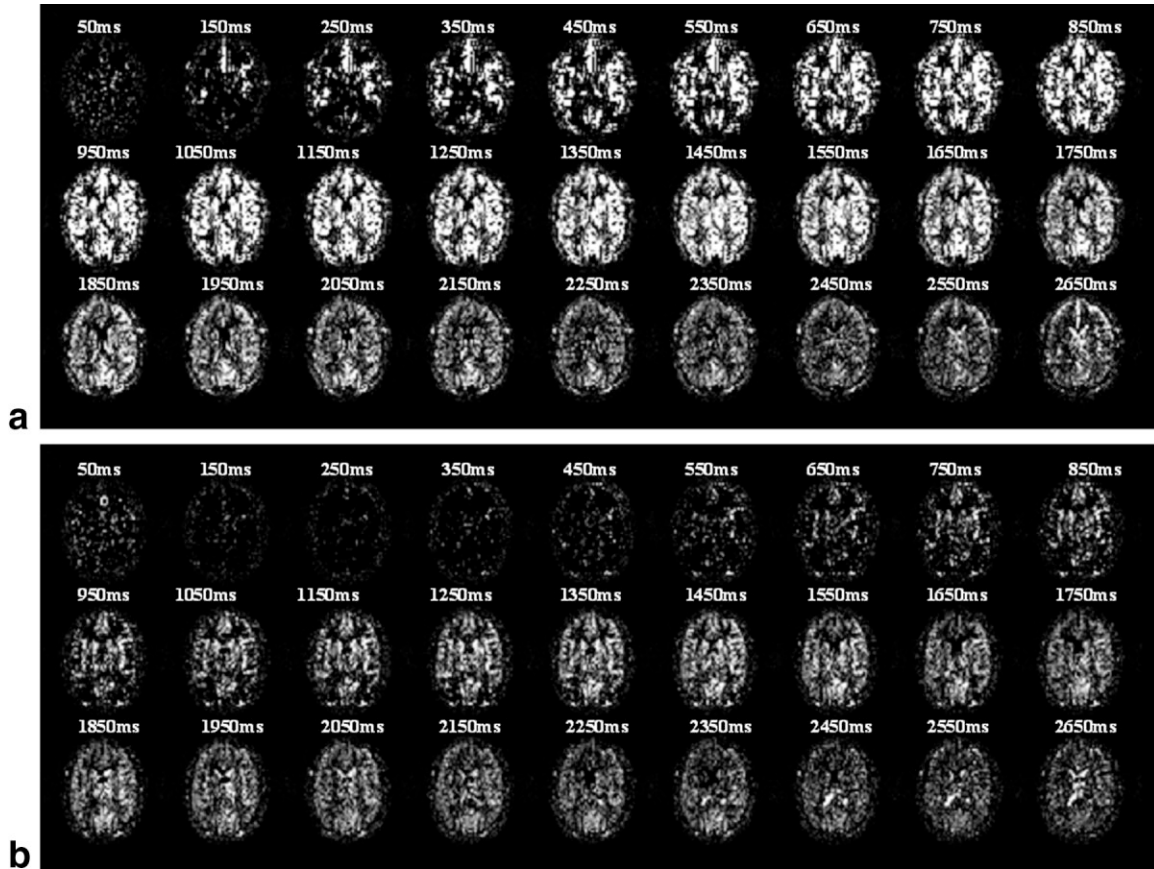
FIG. 1. Multiple time points after labeling of arterial spins in a single-slice of the human brain acquired (**a**) without elimination of the intravascular signal, and (**b**) with elimination of the intravascular signal using a bipolar crusher (V_{enc} = 3 cm/s).

An elegant solution to this problem was formulated by Günther et al. (9), who proposed to measure the ASL signal at multiple inversion times in a single scan by means of a Look-Locker-like readout (20). In that study, absolute CBF was also obtained through the use of an adapted pre-defined model. The general model was modified to accommodate multiple low-flip-angle readouts by substituting R_{1app} in Eq. [4] with $R_{1app,eff} = R_1 + f/\lambda - \ln(\cos\phi)/\Delta TI$ where ϕ is the flip angle, and ΔTI is the interval between the excitation pulses. Hendrikse et al. (21) recently applied a similar scheme using the transfer-insensitive labeling technique (TILT).

However, if we knew the exact shape of the fractional arterial input function $c(t)$, we could perform a deconvolution of Eq. [2] without the need for any assumptions concerning the length of the bolus, the spatial variability of the blood–brain partition coefficient λ, or the number of compartments necessary to fully explain the measured perfusion-weighted signal.

Given that $c(t)$ also describes the inflowing magnetization, we obtain the AIF as measured in a voxel filled with arterial blood if we multiply $c(t)$ by the magnetization difference $2 \cdot M_{0,a}$

$$AIF(t) = 2 \cdot M_{a,0} \cdot c(t) \qquad [5]$$

A deconvolution of the measured perfusion-weighted signal time curve $\Delta M(t)$ by this AIF provides the residue function multiplied by the relaxation function and the perfusion rate:

$$f \cdot R(t - \tau) = f \cdot r(t - \tau) \cdot m(t - \tau) \qquad [6]$$

By definition, the residue function $R(t - \tau)$ is a positive, decreasing function with $R(0) = 1$, and the flow f can be obtained from the maximum of R without any other assumption needed. The only remaining unknown is the AIF itself.

In ASL data, one often sees vascular artifacts associated with inflow of labeled arterial blood into the arteries. In order for Eq. [4] to be valid, there should not be any remaining labeled blood within the vasculature. However, very often, such an assumption cannot be made, because many voxels contain a feeding or traversing artery, which causes substantial overestimation of the perfusion. Ye et al. (22) proposed the use of bipolar crusher gradients to dephase the moving spins in order to eliminate the signal from the large arteries. Two series of such noncrushed and crushed (any spin with a mean velocity > 3 cm/s) ASL data are shown in Fig. 1. The arterial contribution is easily seen, especially in regions with a large number of arteries. Note also the later arrival of the bolus in the crushed ASL series, which is to be expected since these spins must traverse the branching macrovasculature before they reach the tissue where they can exchange. This early vascular

"artifact" in fact holds information about the actual shape of the AIF, even though it is mixed up with the perfusion signal arising from the microvasculature. By subtracting the crushed signal curve from the noncrushed one, one obtains the shape of the AIF; however, this cannot be properly scaled if we do not know the volume fraction of the arterial blood.

Arterial Blood Volume (aBV)

In order to normalize the AIF, both the duration of the label and the value of $M_{o,a}$ must be known, according to Eq. [5]. The duration of the label τ_b is obtained in our case by using a Q2-TIPS-like method (see "Labeling Sequence" above), while $M_{o,a}$ can be estimated from the sagittal sinus, which is the only vessel that is large enough to avoid partial volume effects. The AIF also must be scaled to the correct aBV fraction on a voxel-by-voxel basis, since there will always be partial volume effects at the resolution usually employed in ASL. This can be performed by comparing the area under the local AIF with the calculated bolus area $2 \cdot M_{o,a} \cdot \tau_b$, while taking into consideration the longitudinal relaxation of the blood $T_{1,a}$ during its transit time τ_a. Furthermore, it is important to note that from the arrival of the bolus in a voxel at time τ_a to the arrival in the microvasculature τ_m, the label will experience multiple saturation pulses due to the Look-Locker readout scheme. Therefore, the AIF must be corrected by the factor [9]:

$$\cos^n\phi, \qquad \text{where} \quad n = \text{floor}\left(\frac{\tau_m - \tau_a}{\Delta TI}\right) \qquad [7]$$

Finally, taking the inversion efficiency α into account, $AIF(t)$ can be expressed as

$$AIF(t) = 2 \cdot M_{a,0} \cdot \alpha \cdot \cos^n\phi \cdot c(t) \qquad [8]$$

where

$$c(t) = \left(\frac{(\Delta M_{ncr}(t) - \Delta M_{cr}(t))e^{\frac{1}{T_{1a}}}}{\int_{-\infty}^{\infty}(\Delta M_{ncr}(t) - \Delta M_{cr}(t))e^{\frac{t}{T_{1a}}}dt}\right) e^{\frac{-(1+(\tau_m-\tau_a))}{T_{1a}}} \cdot \tau_b \quad [9]$$

Here, ΔM_{ncr} and ΔM_{cr} are the noncrushed and crushed data, respectively. In our case, α was estimated to be 1.0, and n was calculated by detecting the rising edge of the AIF and the tissue curve to obtain τ_a and τ_m, respectively.

Finally, the area of the local AIF can be calculated and corrected for T_{1a} relaxation of labeled arterial blood. The ratio of this area and the one corresponding to an initially labeled "blood-filled" voxel will give the aBV. Both are calculated as part of the above procedure, and the aBV can be expressed as

$$aBV = \frac{\int_{-\infty}^{\infty}(\Delta M_{ncr}(t) - \Delta M_{cr}(t))e^{\frac{1}{T_{1a}}}dt}{2 \cdot M_{a,0} \cdot \tau_b \cdot \alpha} \qquad [10]$$

Note that the $\cos^n\phi$ factor in Eq. [8] is not present, since it can be assumed that all arterial blood will be renewed between two consecutive excitation pulses.

The use of crushed and noncrushed dynamic ASL data to estimate the aBV was previously suggested by Barbier et al. (23).

MATERIALS AND METHODS

Labeling Sequence

To calculate absolute blood flow by means of deconvolution, one must know the exact temporal length τ_b of the bolus of tagged arterial blood. For this reason we developed a new MRI pulse sequence, named quantitative STAR labeling of arterial regions (QUASAR). It combines a pulsed STAR labeling of arterial regions (PULSAR) labeling technique (7) with a Look-Locker strategy for sampling at multiple time points (20) and a repetitive Q2-TIPS-like bolus saturation scheme for clear definition of the arterial blood bolus (18,19). The general scheme of the QUASAR sequence is depicted in Fig. 2.

The PULSAR labeling scheme is described in detail elsewhere (7). In short, this sequence consists of a multi-slice-capable modified EPI signal targeting by alternating radiofrequency pulses (EPISTAR) sequence (24) that is preceded by an optimized four-pulse water suppression enhanced through T_1-effects (WET) saturation pulse (25), and is followed by an additional saturation pulse, in a manner similar to the QUIPSS I sequence (19) for a clean temporal definition of the start of the bolus. This combination allows the angulation of the labeling slab (green/yellow slab in Fig. 2f) in any direction and therefore permits the selective labeling of individual arteries (7,8). The WET saturation technique was chosen for its insensitivity over a broad range of B_1-field inhomogeneities and T_1 values. Using an interpulse interval of 10 ms and optimizing for $400 \leq T_1 \leq 4200$ ms and $\Delta B_1 = \pm 10\%$, the resulting flip angles were (7): $\theta_1 = 88.9°$, $\theta_2 = 98.7°$, $\theta_3 = 82.5°$, and $\theta_4 = 159.0°$. During the STAR spin preparation, control and labeling pulses are performed at the same location, and to induce identical magnetization transfer effects in both cases, the RF power of the first labeling 180° inversion pulse (green in Fig. 2a–d and f) is counterbalanced using two consecutive adiabatic pulses of half RF power during the control phase, leading to a net 180° + 180° = 0° pulse (yellow in Fig. 2a–c, e, and f). Conventional adiabatic hypersecant pulses are used here (13.3 ms long, with a bandwidth of 1.2 kHz and a B_1 field of 13.5μT and 9.55 μT for the labeling and control experiments, respectively). Finally, to ensure identical timing between both labeling and control experiments, a single 90° dephasing pulse follows the spin preparation phase (blue in Fig. 2b–d and f).

The readout is performed using a conventional multi-slice, single-shot, gradient-echo EPI sequence with a small flip angle. Each slice acquisition is preceded by a bolus saturation in a slab applied inferior to the volume of interest (cyan slab in Fig. 2f) within the period $\tau_b < t < \tau_b\tau_s$ (Fig. 2a). Its width must be chosen according to the time between successive slice acquisitions (typically on the order of 40−60 ms) and the expected speed of the blood in
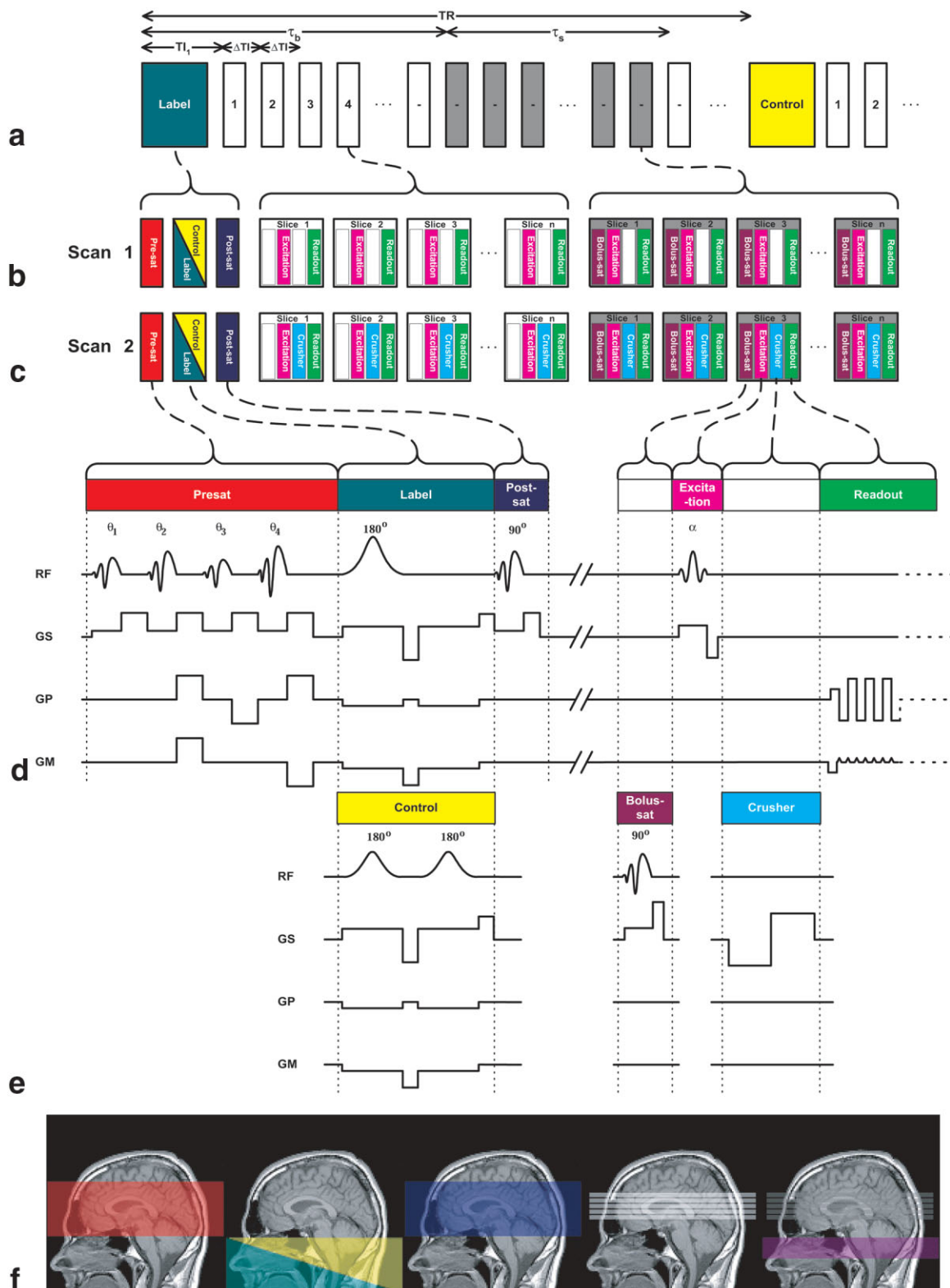
FIG. 2. QUASAR sequence. **a:** The overall structure, showing the spin preparation (labeling/control) followed by the multi-time-point, multislice readout that is interleaved with a bolus saturation sequence for the duration τ_s (shown in gray). τ_b is the temporal length of the labeled bolus. **b** and **c:** The sequence components of the noncrushed and crushed experiments, respectively. **d** and **e:** The actual RF and gradient scheme for presaturation, label/control, postsaturation, bolus saturation, and excitation followed by readout with or without crusher. **f:** (left to right) Presaturation slab, label/control region, postsaturation slab, image acquisition without bolus saturation, and image acquisition with bolus saturation.

order to reach proper bolus saturation (18). More precisely, the bolus saturation must be initiated before the fastest-flowing trailing edge of the tag leaves the inversion region. The duration τ_s during which this saturation is applied should be long enough so that the remaining part of the label will be saturated, but short enough to allow fresh blood to fill up the vessels before the next spin preparation. Finally, the whole experiment is done twice, with (Fig. 2c) and without (Fig. 2b) additional "crusher" or bipolar gradient pulses to allow elimination of the signal from fast-moving spins (22).

MR Experiments

All experiments were performed on a 3.0 T Philips Intera Imager (Philips Medical Systems, Best, The Netherlands) equipped with Master gradients (30 mT/m strength and 120 mT/m/ms slew rate). All images were acquired using the quadrature body coil as transmit coil for optimal B_1 homogeneity, and a dedicated eight-element phased-array receive head coil (MRI Devices Corp., Waukesha, WI, USA).

The experiments were run under a general protocol for pulse-sequence development approved by the local ethics committee, and 13 normal subjects gave written informed consent before they participated in the study. In addition to perfusion ASL experiments, the scan protocol consisted of a conventional localizer, a sensitivity encoding (SENSE) reference scan, and a T_1-weighted image to provide structural information about the location where the perfusion images would be acquired. The QUASAR pulse sequence was performed using the following protocol: four slices; slice thickness = 7 mm; ascending slice order; slice gap = 2 mm; matrix = 64×64; FOV = 240 mm; flip angle = 30°; TR/TE = 4000/23 ms; $TI_1/\Delta TI/\tau_b/\tau_s$ = 50/200/1050/2250 ms; number of acquisition time points = 18; single-shot EPI; SENSE factor = 3.0; inversion slab width = 150 mm; slice/inversion gap = 30 mm; V_{enc} = [∞, 3 cm/s]; and 40 pairs of control and labeled scans for a total scan time of 10 min 40 s. This four-slice protocol forms the basis of the experiments described below, and only the deviations will be mentioned in the following text. In addition to this standard scan, one or more experiments were added per volunteer to test the validity of the various assumptions required by the technique, while keeping the scan time within 1 hr.

The first experiment was designed to optimize the value of the "crusher" gradients. The cutoff velocity of the bipolar gradients was set at six different levels: V_{enc} = ∞, 5, 4, 3, 2, and 1 cm/s. The QUASAR sequence was then run in a single-slice mode, without application of the Q2-TIPS scheme, with ΔTI = 100 ms and 27 acquisition time points repeated 30 times.

The second experiment was performed to validate the assumption that arterial blood is completely renewed between successive excitations. This was done by using different flip angles in the Look-Locker readout scheme, which would vary the level of saturation of the blood remaining in a voxel. This in turn would result in a reduction of the calculated blood volume at high flip angles. Two different protocols were used in this case. In the first one, a single-slice experiment was performed using 10°, 25°, and 60° flip angles with ΔTI = 100 ms, and 26 acquisition time points. This experiment was then repeated in a four-slice protocol that was in all ways similar to the standard one, with two flip angles of 10° and 30°.

In a third experiment the bolus duration τ_b was adjusted for optimum perfusion signal. Images were acquired at four different τ_b's (850, 1050, 1450, and 1850 ms), which made it possible to estimate when the trailing edge of the bolus reached the superior edge of the inversion slab.

The fourth experiment was designed to test the eventual saturation effect experienced by the traversing blood moving from lower to upper slices. It consisted of the standard protocol, although the position of the slices were adjusted in such a way that the lower slice in the second experiment would correspond to the location of the upper slice in the first one, while everything else was kept identical. Analyzing the perfusion values from slice 4 in the first scan, and slice 1 in the second scan provides a means of measuring eventual differences in calculated flow caused by saturation of supplying blood label to the upper slice of the first scan. TI_1 was changed from 50 to 200 ms in the second scan in order to acquire those particular slices at the same TI.

Postprocessing

All images were exported to a Windows PC running IDL 6.0 (Research Systems Inc., Boulder, CO, USA). If necessary, motion correction was performed (26), and pairs of images that showed strong motion artifacts were discarded prior to averaging. The raw images were then modulus-subtracted to produce ΔM images. From these images, two perfusion maps were calculated: one that used the new deconvolution method, and one based on a parameter fit to the modified standard model as described by Günther et al. (9). In particular, for the fitting of $R_{1app,eff}$ and subsequently CBF values, a Levenberg-Marquardt (27) least-squares algorithm was used.

$M_{0,a}$ was measured in a single voxel within the sagittal sinus in the most superior slice to ensure inflow of non-saturated venous blood. To compensate for the differences in R_2^* of venous and arterial blood, and include the expected inversion efficiency, the measured $M_{0,v}$ was multiplied by a conversion factor of 1.73. This factor is based on estimated $R_{2,a}^*$ and $R_{2,v}^*$ values of 18.8 [s^{-1}] and 46.2 [s^{-1}] at 3T (P.C.M. van Zijl, personal communication), as well as a measured inversion efficiency of 0.91 (see "Potential Issues" in the Discussion section).

The relaxation of blood T_{1a} was set to 1650 ms (28). In the case of the standard fit, n in Eq. [7] was chosen to be 2, whereas in the deconvolution method it was calculated on a voxel-by-voxel basis.

Deconvolution

The estimation of the residue function $R(t - \tau)$ and f can be performed using a deconvolution method. However, it is known that in the presence of noise, numerical deconvolution becomes an ill-conditioned problem, and some regularization is needed to achieve stability in order to reach reasonable solutions. By comparing different deconvolution methods for estimating perfusion using DSC tech-

niques, Ostergaard et al. (12) found the singular value decomposition (SVD) technique to be stable even at relatively low SNR. The nature of the subtracted perfusion signal in an ASL experiment is very similar to the one obtained using contrast agents, although the bolus duration and sampling rate both differ. The discretized form of the deconvolution can be written as:

$$\Delta M(t_j) = \Delta TI \cdot f \cdot \sum_{i=0}^{j} AIF(t_i) \cdot R(t_j - t_i) \qquad [11]$$

By expanding it into matrix notation:

$$
\begin{bmatrix}
\Delta M(t_0) \\
\Delta M(t_1) \\
\vdots \\
\Delta M(t_{N-1})
\end{bmatrix}
$$

$$
= \Delta TI \cdot f \cdot
\begin{bmatrix}
A1F(t_0) & 0 & \cdots & 0 \\
A1F(t_1) & A1F(t_0) & \cdots & \vdots \\
\vdots & \vdots & \ddots & \vdots \\
A1F(t_{N-1}) & A1F(t_{N-1}) & \cdots & A1F(t_0)
\end{bmatrix}
$$

$$
\times
\begin{bmatrix}
R(t_0) \\
R(t_1) \\
\vdots \\
R(t_{N-1})
\end{bmatrix}
\qquad [12]
$$

The solution of the above equation can be obtained using SVD. A straightforward method of regularization, known as truncated SVD, is to threshold the singular values obtained by this algorithm, neglecting smaller values below a preset tolerance. This will in turn stabilize the system by lowering its rank. The flow *f* can then be obtained from the maximum of *R*. However, this method has been shown to be sensitive to both dispersion and delay. Wu et al. (29) proposed a modified version of the truncated SVD using a block-circulant deconvolution matrix that is insensitive to these effects, known as "circular SVD." This method was chosen for the computation in our case and was implemented using the SVDC algorithm (30).

Local AIF Selection

Localized AIFs were selected on the basis of aBV. Typically, voxels with more than 1.2% aBV were selected to avoid using ill-defined AIFs. The Euclidean distance was then calculated between any voxel to the nearest valid AIF. If more than one AIF was found at the same distance, the averaged AIF was then used to further calculate the perfusion.

Edge Detection

To scale the AIF correctly, the onsets of the AIF (τ_a) and of the tissue curve (τ_m) must be assessed. To measure these onsets, we used the edge detection algorithm originally proposed by Canny (31). In its actual implementation, the perfusion-weighted signal is first convolved with a Gaussian function and subsequent maxima are detected using a partial derivative of the resulting signal. The derivative is calculated by convolution with a standard Sobel kernel.

Simulations

The SVD deconvolution method and the Levenberg-Marquardt least-squares fit were tested to estimate their respective performance in the flow range of 10–150 ml/100 g/min at SNR levels of ∞, 15, 10, and 5. This was done mainly to estimate potential systematic errors, and was not intended to be a study of algorithm performance. A total of 5000 repetitions were carried out for each combination using a Monte Carlo approach. The input function was convolved by a Gaussian dissipation (32), and the standard fast-exchange Kety model was used for the vascular kinetics (6,9). Data were simulated with a sampling rate of 200 ms and 18 time points, similarly in all ways to our standard scan protocol.

An additional simulation was performed to test the potential error made by extracting AIFs from modulus instead of complex subtraction of labeled from control scans. This error may be more important in vessels that show a large arterial fraction. Therefore, a simulation of the error made in a voxel filled with 20% arterial volume was carried out. For both simulations, tissue and blood relaxation T_1 and $T_{1,a}$ were set to 1.1 s and 1.65 s, respectively.

RESULTS

Simulations

Figure 3 shows the results from the Monte Carlo simulations, in which estimated flow vs. true flow values are plotted for different SNRs. The simulated mean flow values using the SVD method are shown as filled circles in Fig. 3, while values calculated using the standard kinetic model are shown as open circles. Note that only half of the standard deviation (SD) is plotted in each case. Table 1 shows simulated flow estimates at three different values (30, 60, and 90 ml/100 g/min) that match white matter (WM) and low and high gray matter (GM) values, respectively, and for each SNR level (∞, 15, 10, and 5). For instance, in the case of 60 ml/100 g/min and SNR = 10, the simulated flow values were 50 ± 11 and 64 ± 27 (mean ± SD) for the deconvolution approach and parameter fit, respectively. This corresponds to a deviation of –17% and 7% from the true flow for deconvolution and fit, respectively.

Figure 4 demonstrates the potential error that can be made when a modulus-subtraction of the arterial signal (as performed in our case) is used instead of a correct complex subtraction. It can be seen that the error is very small and concerns primarily the first ~200 ms after the labeling.

MR Experiments

Perfusion maps were obtained in all 13 volunteers. The perfusion values are summarized in Table 2. The averaged CBF values across subjects were 32 ± 1, 38 ± 2, and 23 ± 1 ml/100 ml/min (mean ± SEM) for total matter, GM, and WM, respectively, using the deconvolution method, and 38 ± 2, 42 ± 2, and 34 ± 1 ml/100 ml/min, respectively, when fitted to the standard kinetic model. The averaged aBV values were 0.81% ± 0.04%, 0.93% ± 0.06%, and 0.33% ± 0.02% (mean ± SEM) for total matter, GM, and WM, respectively, among all subjects. Figure 5 shows a
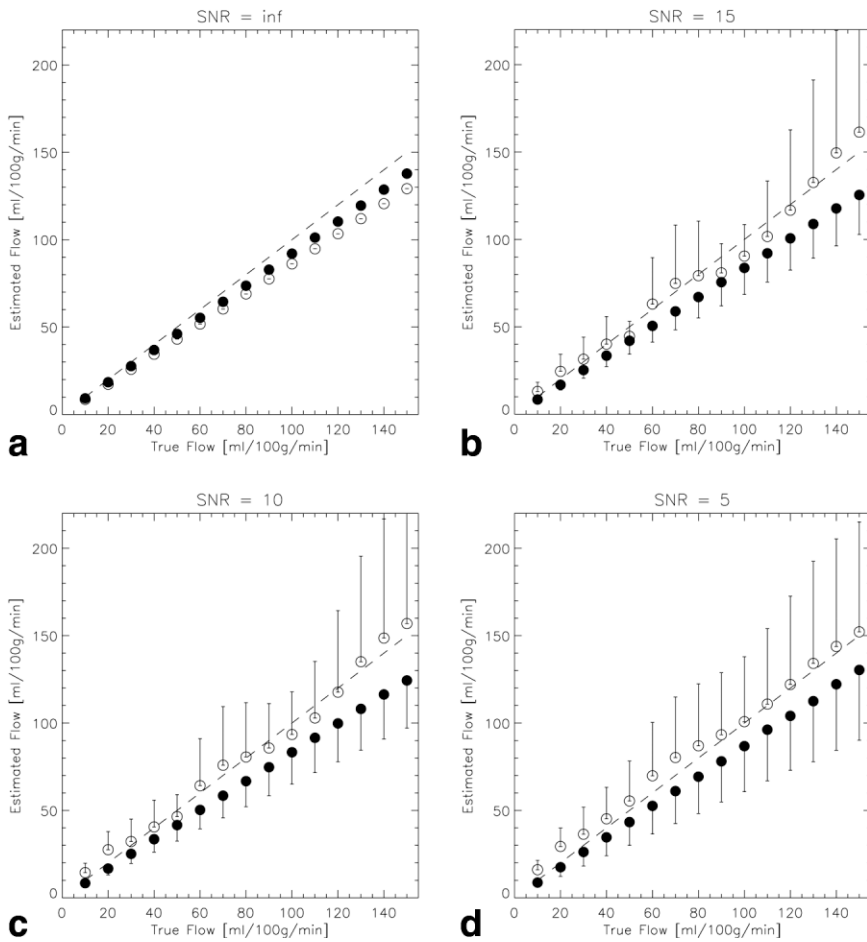
FIG. 3. Monte Carlo simulations of the flow estimate using deconvolution (filled circles) or traditional fit (open circles): (**a**) no noise, (**b**) SNR = 15, (**c**) SNR = 10, and (**d**) SNR = 5. Simulated data using 5000 repetitions of the standard Kety model with a boxcar function convolved with a Gaussian dissipation as input function. Simulation parameters: tissue relaxation $T_1 = 1.1$ s, blood relaxation $T_{1,a} = 1.65$ s, blood-tissue partition coefficient $\lambda = 0.9$, flip angle $\phi = 30°$, $\Delta T = 200$ ms, and 18 sample points. Mean values and SDs in one direction are plotted.

deconvolved CBF-map (a), fitted CBF-map (b), aBV-map (c), and fitted $R_{1app,eff}$ map (d) of a representative volunteer.

From the results of the first experiment aimed at selecting an appropriate crusher level for our scan protocol, the flow was measured by fitting the perfusion-weighted signal using the standard kinetic model. The resulting flow distributions for GM at different crusher gradients levels are shown in Fig. 6, while image time series from this experiment are displayed in Fig. 1. The mean calculated CBF values were 108 ± 130 ml/100 ml/min, 49 ± 27 ml/100 ml/min, 54 ± 29 ml/100 ml/min, 47 ± 28 ml/100 ml/min, 41 ± 23 ml/100 ml/min, and 39 ± 26 ml/100 ml/min (mean $\pm$ SD) for crusher levels of $V_{enc} = \infty$, 5, 4, 3,

2, and 1 cm/s, respectively. For segmentation, voxels were considered as belonging to GM if their $R_{1app,eff}$ was within the range of 0.6–1.2 s^{-1} ($T_{1app,eff} = 0.83$–1.67s), and likewise WM voxels consisted of those within the range of $R_{1app,eff} = 1.2$–2.0 s^{-1} ($T_{1app,eff} = 0.5$–0.83 s). This segmentation was based on the histogram of $R_{1app,eff}$ values of all volunteers. It was used for all experiments.

In the first part of the second experiment, the GM aBV at different flip angles was measured to be $1.04\% \pm 1.68\%$, $0.75\% \pm 1.16\%$, and $0.52\% \pm 1.21\%$ (mean $\pm$ SD) for flip angles of $10°$, $25°$, and $60°$, respectively, corresponding to a reduction of 20% and 50% of aBV at $25°$ and $60°$ with respect to $10°$. These were acquired with a slice thickness of 7 mm and a ΔTI of 100 ms. In another volunteer, the

Table 1
Flow Estimates Using Monte Carlo Simulations for Deconvolution (CBF$_1$) and Fit to the Standard Model (CBF$_2$)*

SNR	CBF$_1$ [mL/100 mL/minute]			CBF$_2$ [mL/100 mLl/minute]		
	30	60	90	30	60	90
∞	28 ± 0	55 ± 0	83 ± 0	26 ± 0	52 ± 0	78 ± 0
15	25 ± 5	51 ± 9	76 ± 14	31 ± 13	63 ± 27	81 ± 17
10	25 ± 5	50 ± 11	75 ± 16	32 ± 13	64 ± 27	86 ± 25
5	26 ± 8	53 ± 16	78 ± 23	36 ± 15	70 ± 31	93 ± 35

*Values for each combination ($n = 5000$) are mean $\pm$ SD. Simulation parameters: Tissue relaxation $T_1 = 1.1$ s, blood relaxation $T_{1,a} = 1.65$ s, blood-tissue partition coefficient $\lambda = 0.9$, flip angle $\phi = 30°$, $\Delta T = 200$ ms and 18 sample points.
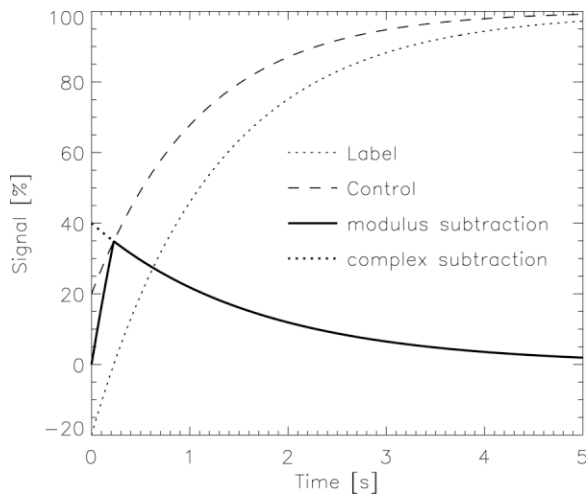
FIG. 4. Effects of modulus subtraction of the labeled and control images for the AIF are simulated in the case of 20% aBV in a voxel. The label and control relaxation curves are plotted for tissue and blood relaxation T_1 and $T_{1,a}$ = 1.1 s and 1.65 s, respectively. The AIF curves simulated for modulus and complex acquisition are shown.

same slice thickness was used, but with a ΔTI of 200 ms at 10° and 30°, giving aBV values of 0.69% ± 1.39% and 0.75% ± 1.50%, respectively.

The mean aBV values from the third experiment were 0.75% ± 1.50%, 0.69% ± 1.44%, 0.68% ± 1.09%, and 0.64% ± 0.98% (mean ± SD) for bolus durations τ_b of 850, 1050, 1450, and 1850 ms, respectively.

Saturation effects on traversing blood supplying superior slices resulted in the following CBF values: 28 ± 16 ml/100 ml/min, 36 ± 12 ml/100 ml/min, and 19 ± 10 ml/100 ml/min (mean ± SD) for total matter, GM, and WM, respectively, for the fourth slice of scan 1. On the other hand, the lowest slice of scan 2 resulted in the following CBF values: 27 ± 18 ml/100 ml/min, 35 ± 11 ml/100 ml/min, and 23 ± 13 ml/100 ml/min (mean ± SD).

DISCUSSION

Simulations

From Fig. 3a–d it can be seen that the SVD algorithm has a tendency to underestimate the flow, while values calculated using the standard kinetic model seem to be more in line with the true flow values. An exception to this is infinite SNR, in which case the SVD actually performs better.

In general, the SDs of the fits are larger than those obtained by SVD, especially in the physiologically relevant range of 0–80 ml/100 g/min. However, this difference depends on the priority of the methods used (i.e., whether accuracy or precision is favored). In the present simulations the fit showed a higher accuracy but a lower precision compared to the SVD method. For instance, if an SVD threshold that resulted in a more accurate mean CBF were chosen, it would be at the expense of a lower precision.

A certain underestimation of the flow by SVD is expected because regularization is known to underestimate flow, as is also seen in DSC-MRI and similar applications (29). Furthermore, it should be kept in mind that the data were simulated using the fast-exchange model, and the fit algorithm was fed with the true $T_{1app,eff}$, which induced some bias between both methods.

As regards the use of modulus instead of complex subtraction for AIF extraction, it can be seen from Fig. 4 that even in the case of 20% of aBV in a voxel, which occurs only rarely at our resolution (voxel volume = 98 mm³), the effect will not persist after approximately 200–300 ms. Since our first sampling time is at 50 ms, when the blood has not yet flowed through the 30-mm gap between the labeling and the image plane, and the second sample is acquired 200 ms later, this phenomenon is unlikely to affect our data analysis.

Optimized Crusher Size

From the mean CBF values, as well as the histogram in Fig. 6, it can be seen that without bipolar crusher gradients, the

Table 2
Flow Estimates from 13 Subjects, Using Deconvolution (CBF$_1$) and Fit to the Standard Model (CBF$_2$) as well as Arterial Blood Volume (aBV)*

Subject	CBF$_1$ [ml/100 ml/min]			CBF$_2$ [ml/100 ml/min]			aBV [%]		
	Total	GM	WM	Total	GM	WM	Total	GM	WM
1	29	35	19	36	39	31	0.87	1.04	0.35
2	33	38	22	42	47	37	0.75	0.81	0.29
3	32	38	21	37	42	32	0.81	0.75	0.23
4	27	35	18	32	38	27	0.81	0.98	0.35
5	36	45	25	39	44	36	1.10	1.39	0.46
6	27	34	18	36	41	34	0.69	0.87	0.40
7	35	42	25	42	47	36	0.81	0.98	0.29
8	30	38	21	36	42	29	0.75	0.98	0.35
9	34	26	18	23	24	30	0.87	0.52	0.35
10	39	47	28	44	51	38	0.98	1.10	0.35
11	32	36	26	35	39	34	0.58	0.69	0.29
12	39	49	29	49	56	44	0.75	0.92	0.29
13	27	31	23	35	36	36	0.81	1.10	0.35
Total	32 ± 1	38 ± 2	23 ± 1	37 ± 2	42 ± 2	34 ± 1	0.81 ± 0.04	0.93 ± 0.06	0.33 ± 0.02

*Voxels were considered to be in the gray matter (GM) and white matter (WM), respectively, if their $T_{1app,eff}$ was: GM = 0.83 < $T_{1app,eff}$ < 1.63s, WM = $T_{1app,eff}$ < 0.83. Values are mean/(mean ± SEM).
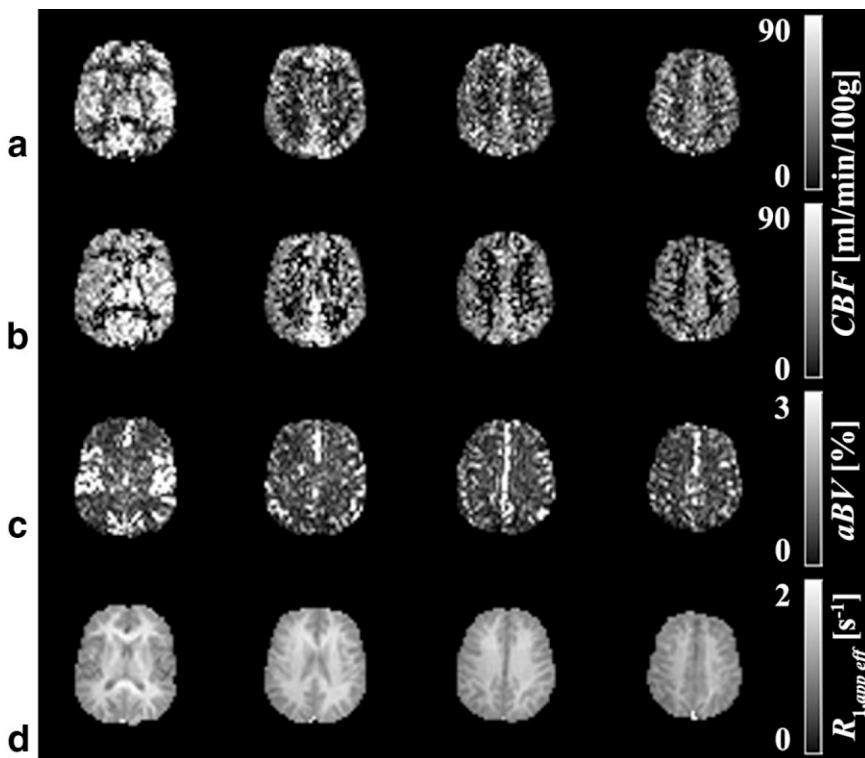
FIG. 5. Estimated perfusion (CBF) maps of a representative volunteer using (**a**) deconvolution and (**b**) three-parameter fit. **c:** aBV map. **d:** Fitted $R_{1app,eff}$ map.

general kinetic model will lead to gross overestimation of the perfusion values. This is a common problem that is linked to the acquisition of a train of observations after a single spin preparation sequence (9,21). In single time-point ASL studies, this phenomenon is less pronounced because the inversion time is often chosen in the range of 1.2–1.7 s, which suppresses the inflow effect that is present at short inversion times. Thus, it can be noted that the application of even small gradients of $V_{enc} = 5$ cm/s

narrows the flow distribution to more physiologically reasonable values. Even more interesting is the observation that the flow distribution does not change considerably even when crusher gradients are increased to $V_{enc} = 1$ cm/s, which corresponds to a diffusion weighting of $b = 8.8$ s/mm^2. This observation implies that the gain in flow accuracy by selecting very small V_{enc} values, which ideally could be only slightly higher than the expected blood velocity of 0.2–5.0 mm/s in the capillary bed, would be canceled out by extended TE and decreased SNR. Therefore, a crusher gradient corresponding to $V_{enc} = 3$ cm/s ($b = 1.7$ s/mm^2) was chosen as a trade-off.

Validation of the Assumptions

Results from the experiment with varying flip angles show that in the case of a 7-mm slice thickness and a sampling rate of 100 ms, saturation of the arterial blood occurs within the slice. It can be concluded that the labeled blood in the larger arteries is not refreshed between two consecutive excitations, which in turn gives rise to underestimated aBV. This can be solved by decreasing either the slice thickness or the sampling rate. To maintain the SNR, we reduced the sampling rate to 200 ms. The second experiment shows similar values for flip angles of 10° or 30°, indicating that the assumption of refreshment of labeled blood between excitations can be considered fulfilled in that volunteer. The lower sampling rate is in any case necessary for multislice acquisition. However, in general, ΔTI and the slice thickness should be chosen carefully to avoid saturation of feeding or traversing blood vessels. For example, this is especially important for elderly patients with compromised arterial blood circulation. Moreover, in cases in which very low perfusion oc-
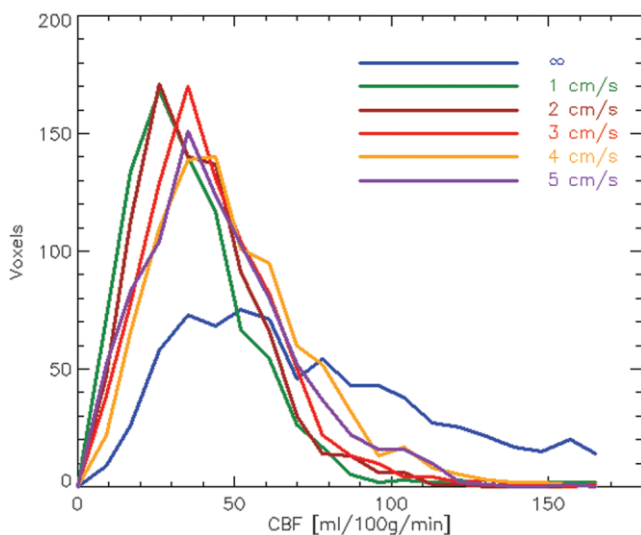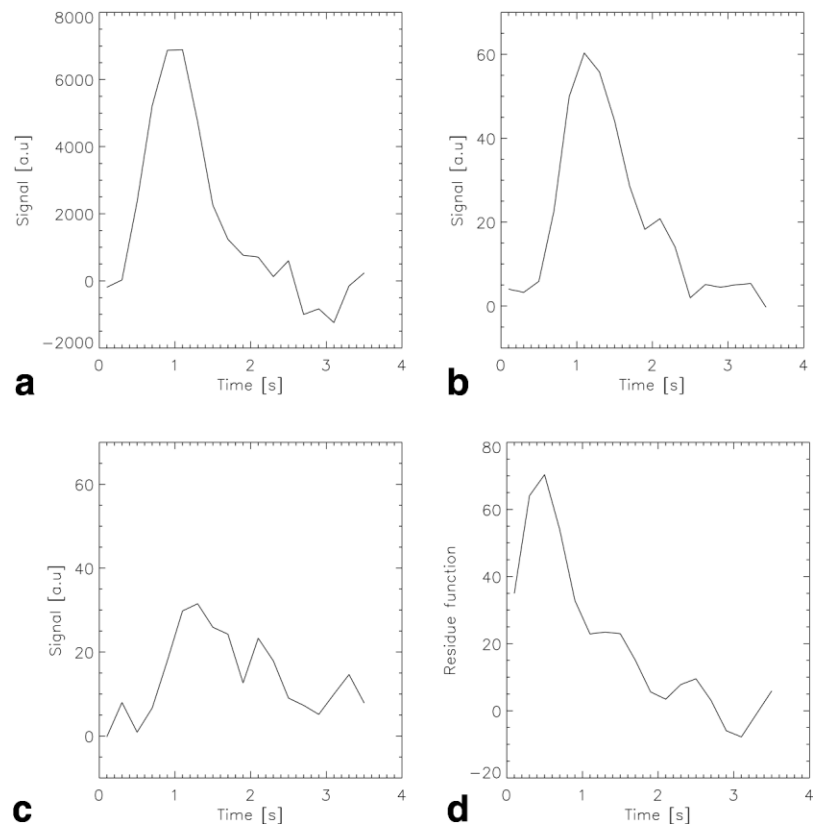

FIG. 6. Flow distribution from fitted GM perfusion at five velocity encoding levels. Intra-arterial flowing blood signal was eliminated by the use of bipolar gradients ($V_{enc} = \infty$, 5, 4, 3, 2 and 1 cm/s) prior to readout.

FIG. 7. (**a**) Typical AIF measured in the GM, and tissue curves from (**b**) GM and (**c**) WM. **d:** The resulting residue function for the GM curve corresponding to a flow of 70 ml/100 g/min.

curs, this can potentially affect the local aBV estimation, whereas the AIFs used for perfusion quantification are chosen according to a minimum aBV. If this minimum value is attained, it means that the mean velocity of the arterial blood is higher than or equal to the chosen velocity encoding used for the crushers, and refreshing of the labeled blood can therefore be ensured.

For absolute flow quantification, we need to be certain that the decided bolus duration is obtainable. In particular, the fastest-flowing blood in the bolus should not leave the labeling region before the saturation pulse train is applied. In the original Q2-TIPS paper (18), the time before arrival of the trailing edge of a 10-cm inversion slab was estimated to be around 700 ms. The present protocol instead uses an inversion slab of 15 cm, thereby extending the bolus duration. The mean aBV values from the third experiment were all within the range of error for bolus durations τ_b of up to 1450 ms, while they started to decrease at $\tau_b = 1850$ ms. Therefore, to ensure a clear bolus definition in all subjects, a conservative bolus duration of 1050 ms was chosen for the experiments.

Saturation effects on traversing blood supplying superior slices were negligible with a total mean CBF value of 28 ± 16 vs. 27 ± 18 ml/100 ml/min (mean $\pm$ SD) for the case of possible saturation (using the upper slice of a four-slice experiment) and the one without (using the lowest acquired slice). Therefore, this effect apparently does not impair our results in a first approximation.

Comparison of the General Kinetic Model and Deconvolution

Generally, our method provided CBF values that were 10% lower than those obtained using the general kinetic model, although both values fall within the range of published literature (9,21,33). Figure 7a shows a typical AIF measured in the GM. Tissue curves from GM and WM are shown in Fig. 7b and c, respectively. The resulting residue function for the GM area is shown in Fig. 7d, and in this particular case it corresponds to a perfusion of 70 ml/100 g/min. There could be several reasons for this difference. The deconvolution method is known to underestimate the true flow (12,29,34–36), as also shown in Fig. 3 using our Monte Carlo analyses. The fitting to the general model assumes a typical boxcar AIF shape and uses the solution for a single compartment. Eventual violation of one or more of these assumptions can change the final estimate in either direction. However, the error is less than that predicted by the Monte Carlo simulations, where an underestimation of 17% was shown at a true flow of 60 ml/100 g/min. This better performance could reflect the fact that the distribution of the real AIF is more dispersed than the one used for the simulations, which would influence both the fit and deconvolution.

Another difference is the GM/WM ratio: while the deconvolution methods yield a ratio of 1.7, the three-parameter fit yields a relatively smaller ratio of 1.2. This overestimation of CBF in WM is typical of a three-parameter fit, which will try to fit a curve to even very poor SNR data, as are sometimes found in WM. In that regard the SVD method is less sensitive, since such low SNR data will only be scaled to the maximum of the residue function without additional extrapolation.

Generally, a difference of 10% seen in relation to the available SNR in ASL data will be within the range of error, and further optimization of both methods might narrow that difference. The SVD algorithm is known to be

a robust regularization tool, and hence this approach was chosen for these preliminary tests. In future studies, other methods (e.g., Wiener-filtered-Fourier methods or the expectation-maximization method) could be tested for their performance in this particular application (11,37). To further validate the new approach, comparisons with other modalities (e.g., DSC-MRI and PET) are needed.

Having acquired the AIF, another way to analyze the data could be to convolve the AIF with an exponential residue function, as used in the standard model. This could then be used as an input to the fitting algorithm, which would avoid the inversion problem. However, the residue function must be assumed, and the T_1 or $T_{1app,eff}$ would have to be measured, which would introduce additional errors.

Nonetheless, we believe our approach is well suited for quantitative perfusion imaging because the AIF is measured within or in the vicinity of the voxel, and kinetic assumptions about fast or intermediate exchange rates between multiple compartments can be avoided. In relation to other deconvolution-based methods, such as DSC-MRI (12) or CT perfusion (11), the fact that no partial volume effects occur when the local AIF time curves are selected in the ASL approach is a clear advantage. Furthermore, in DSC-MRI, for instance, assumptions about the linear relationship between $\Delta R_2(t)$ and the contrast concentrations must be made. This is contrary to ASL, where a direct linear relationship exists between labeled spins and the observed perfusion signal.

aBV

The average aBV of 0.81% (shown in Table 2) is in line with values published recently by An and Lin (38), who reported a total blood volume of 3.2% and a venous to total blood volume ratio of 0.77. In our case, such a ratio would give a total CBV of 3.5%. The GM blood volume would then be 4.0%, in agreement with earlier PET measurements (39). It can be seen from Fig. 5c that the larger blood volumes are seen at the periphery of the cortex, or where large arteries intersect with the measured slice, in accordance with anatomical knowledge. The WM aBV was 0.3%, and as a result of the small aBV in WM, the signal differences between the curves measured in the crushed and noncrushed scans are small. Therefore, the AIFs used in WM were usually taken from the surrounding GM regions.

Potential Issues

ASL methods rely on correct measurements of the arterial blood equilibrium magnetization $M_{0,a}$ to calculate absolute quantitative perfusion. However, in practice it is difficult to find arterial vessels that are totally filled with blood; hence, in this study the same value was taken for both methods from the sagittal sinus, where chances that the surrounding tissue will give rise to partial volume effect are minimal but still potentially present. It should be noted that although ideally the $M_{0,a}$ is determined, we instead measured $M_{0,v}$, which can differ due to differences in T_2^* between deoxygenated and oxygenated blood. Silvennoinen et al. (40) investigated the dependence of blood

R_2 and R_2^* at different field strengths and showed that blood relaxation parameters relate parabolically to the oxygenation saturation fraction Y:

$$R_2^* = A^* + B^*(1 - Y) + C^*(1 - Y)^2 \qquad [13]$$

where A^*, B^*, and C^* were measured to be 18, 39, and 119, respectively, at 3T, and for a hematocrit fraction of 0.44 (P.C.M. van Zijl, private communication). In gradient-echo acquisitions, this would therefore lead to a rather large underestimation of $M_{0,a}$ depending on the TE selected. For this reason, the value for $M_{0,v}$ was corrected in the present study using Eq. [13].

In fact, by assuming 98% and 65% oxygen saturation for arterial and venous blood respectively, Eq. [13] predicts $R_{2,a}^*$ and $R_{2,v}^*$ values of 18.8 [s^{-1}] and 46.2 [s^{-1}], respectively. In the current study, if a TE of 23 ms was used this would cause an underestimation of $M_{0,a}$ by a factor of 1.9. Furthermore, to verify the actual inversion efficiency of our method, we performed a high-resolution scan on a single volunteer covering the internal carotid artery and the jugular vein (data not shown). The inversion efficiency was measured to be 0.91, which is to be expected given the double inversion of the control scan.

Furthermore, the typical voxel resolution of 3.75 $\times$ 3.75 $\times$ 7.00 mm^3 could introduce partial volume effects within the sagittal sinus, which could also influence the estimation of $M_{0,a}$. By measuring the sagittal sinus on high-resolution magnetization prepared rapid acquisition gradient-echo (MPRAGE) images of a few volunteers ($N = 3$, data not shown), the sagittal sinus could be approximated by an equal-sided triangle (1.1 cm on the lateral sides, and 0.95 cm on the posterior side) in the region where $M_{0,v}$ was extracted. Compared to the present voxel size, this could introduce partial volume effects from zero to a few percent depending on the angulations of the slices. Although in the present study we assumed that no partial volume effects were present, we realize that better ways to estimate $M_{0,a}$ are needed, since it is the most important scaling factor in any ASL experiment.

Based on the above discussion, an overall correction factor of 1.9 $\times$ 0.91 = 1.73 was multiplied to the measured $M_{0,v}$ values before flow calculation to compensate for nonideal inversion and R_2^* differences.

Finally, it should be noted that in this study the estimated $M_{0,a}$ was used for both the deconvolution and the traditional model fit, and since it is a direct scaling factor, an eventual error in the estimate will not affect the comparison of the two methods. While both values are on the lower end of what has been published in the ASL literature, they are close to the values (CBF_{GM} = 42 ml/min/100 g) obtained using a similar acquisition technique (21). Also, whereas most estimated GM and WM values are often based on hand-drawn ROIs on CBF maps, and are therefore prone to bias, in the present study we used an automatic segmentation procedure, which provided unbiased but possibly less precise estimations of GM and WM perfusion values. An additional factor that influences the perfusion estimate is the estimated blood T_1. In this study, for both fit and deconvolution methods, an overestimation of blood T_1 by 10% was found to cause an underestimation of the perfusion by 10% (simulations not shown).

Furthermore, the fact that the crusher scheme used in this study was limited to a unique spatial direction could introduce some errors into the perfusion estimation. For instance, when crusher gradients were applied in the slice-selection direction, only the velocity components that were perpendicular to the image plane were spoiled. Feeding arteries parallel to the image plane would not have been crushed, and could have introduced errors in the perfusion estimate. Future improvements should therefore include the implementation of crushers in all directions to eliminate this phenomenon.

Like other acquisition schemes and models, this model-free approach also suffers from intrinsic errors in the acquisition. These originate from the sensitivity of the scanner at the voxel level, where differences in T_2 and T_2^* of the tissue affect the MR signal depending on the coil and TE used.

Finally, another possible problem could arise from the fact that the crushed experiments are acquired using a diffusion gradient, which would add a diffusion weighting to the image, in addition to eliminating the signal from fast-flowing blood. However, when using bipolar crusher gradients of $V_{enc} = 3$ cm/s or $b = 1.7$ s/mm^2 and assuming a GM diffusion coefficient D of $0.8 \cdot 10^{-3}$ mm^2/s, the resulting effect contributes to a $<0.14\%$ signal drop in the GM: $\Delta s \propto (1 - e^{-b \cdot D}) \cdot 100\% = 0.14\%$, which is negligible compared to an expected signal change of 1–2% due to perfusion. The subtraction control label should further eliminate eventual differences as compared to the non-crushed experiment.

CONCLUSIONS

In the present work a robust, model-free method for absolute quantification of CBF was developed based on an SVD-based deconvolution technique. A new pulse sequence was also implemented that allowed independent measurement of the AIF on a voxel-by-voxel basis. The method was evaluated on 13 healthy volunteers, and the measured perfusion was in good agreement with the literature. This new approach provided lower CBF values than those obtained using the standard kinetic model in accordance with Monte Carlo simulations. However, quantification issues, such as accurate extraction of the equilibrium magnetization of blood, remain to be addressed in order to ensure reproducible and absolute quantification of CBF.

ACKNOWLEDGMENTS

REFERENCES

1. Golay X, Hendrikse J, Lim TC. Perfusion imaging using arterial spin labeling. Top Magn Reson Imaging 2004;15:10–27.
2. Kim SG, Tsekos NV. Perfusion imaging by a flow-sensitive alternating inversion recovery (FAIR) technique: application to functional brain imaging. Magn Reson Med 1997;37:425–435.
3. Salmeron BJ, Stein EA. Pharmacological applications of magnetic resonance imaging. Psychopharmacol Bull 2002;36:102–129.
4. Kety SS, Schmidt CF. The nitrous oxide method for the quantitative determination of cerebral blood flow in man: theory, procedure and normal values. J Clin Invest 1948;4:476–483.
5. Williams DS, Detre JA, Leigh JS, Koretsky AP. Magnetic resonance imaging of perfusion using spin inversion of arterial water. Proc Natl Acad Sci USA 1992;89:212–216.
6. Buxton RB, Frank LR, Wong EC, Siewert B, Warach S, Edelman RR. A general kinetic model for quantitative perfusion imaging with arterial spin labeling. Magn Reson Med 1998;40:383–396.
7. Golay X, Petersen ET, Hui F. Pulsed star labeling of arterial regions (PULSAR): a robust regional perfusion technique for high field imaging. Magn Reson Med 2004;53:15–21.
8. Hendrikse J, van der Grond J, Lu H, van Zijl PC, Golay X. Flow territory mapping of the cerebral arteries with regional perfusion MRI. Stroke 2004;35:882–887.
9. Günther M, Bock M, Schad LR. Arterial spin labeling in combination with a Look-Locker sampling strategy: inflow turbo-sampling EPI-FAIR (ITS-FAIR). Magn Reson Med 2001;46:974–984.
10. Meier P, Zierler KL. On the theory of the indicator-dilution method for measurement of blood flow and volume. J Appl Physiol 1954;6:731–744.
11. Gobbel GT, Fike JR. A deconvolution method for evaluating indicator-dilution curves. Phys Med Biol 1994;39:1833–1854.
12. Ostergaard L, Weisskoff RM, Chesler DA, Gyldensted C, Rosen BR. High resolution measurement of cerebral blood flow using intravascular tracer bolus passages. I. Mathematical approach and statistical analysis. Magn Reson Med 1996;36:715–725.
13. Kim SG. Quantification of relative cerebral blood-flow change by flow-sensitive alternating inversion-recovery (FAIR) technique—application to functional mapping. Magn Reson Med 1995;34:293–301.
14. Kwong KK, Chesler DA, Weisskoff RM, Donahue KM, Davis TL, Ostergaard L, Campbell TA, Rosen BR. MR perfusion studies with T$_1$-weighted echo-planar imaging. Magn Reson Med 1995;34:878–887.
15. Calamante F, Williams SR, van Bruggen N, Kwong KK, Turner R. A model for quantification of perfusion in pulsed labelling techniques. NMR Biomed 1996;9:79–83.
16. St Lawrence KS, Frank JA, McLaughlin AC. Effect of restricted water exchange on cerebral blood flow values calculated with arterial spin tagging: a theoretical investigation. Magn Reson Med 2000;44:440–449.
17. Zhou J, Wilson DA, Ulatowski JA, Traystman RJ, van Zijl PC. Two-compartment exchange model for perfusion quantification using arterial spin tagging. J Cereb Blood Flow Metab 2001;21:440–455.
18. Luh WM, Wong EC, Bandettini PA, Hyde JS. QUIPSS II with thin-slice TI$_1$ periodic saturation: a method for improving accuracy of quantitative perfusion imaging using pulsed arterial spin labeling. Magn Reson Med 1999;41:1246–1254.
19. Wong EC, Buxton RB, Frank LR. Quantitative imaging of perfusion using a single subtraction (QUIPSS and QUIPSS II). Magn Reson Med 1998;39:702–708.
20. Gowland P, Mansfield P. Accurate measurement of T$_1$ in-vivo in less than 3 seconds using echo-planar imaging. Magn Reson Med 1993;30:351–354.
21. Hendrikse J, Lu HZ, van der Grond J, van Zijl PCM, Golay X. Measurements of cerebral perfusion and arterial hemodynamics during visual stimulation using Turbo-TILT. Magn Reson Med 2003;50:429–433.
22. Ye FQ, Mattay VS, Jezzard P, Frank JA, Weinberger DR, McLaughlin AC. Correction for vascular artifacts in cerebral blood flow values measured by using arterial spin tagging techniques. Magn Reson Med 1997;37:226–235.
23. Barbier EL, Silva AC, Kim SG, Koretsky AP. Perfusion imaging using dynamic arterial spin labeling (DASL). Magn Reson Med 2001;45:1021–1029.
24. Edelman RR, Chen Q. EPISTAR MRI: multislice mapping of cerebral blood flow. Magn Reson Med 1998;40:800–805.
25. Ogg RJ, Kingsley PB, Taylor JS. WET, a T$_1$- and B_1-insensitive water-suppression method for in vivo localized 1H NMR spectroscopy. J Magn Reson B 1994;104:1–10.
26. Woods RP, Grafton ST, Holmes CJ, Cherry SR, Mazziotta JC. Automated image registration: I. General methods and intrasubject, intramodality validation. J Comput Assist Tomogr 1998;22:139–152.
27. Moré JJ. 1978. The Levenberg-Marquardt algorithm: implementation and theory. In: Watson GA, editor. Lecture Notes in Mathematics 630. Berlin: Springer-Verlag. p. 105–116.

28. Lu H, Clingman C, Golay X, van Zijl PC. Determining the longitudinal relaxation time (T_1) of blood at 3.0 Tesla. Magn Reson Med 2004;52:679−682.

29. Wu O, Ostergaard L, Weisskoff RM, Benner T, Rosen BR, Sorensen AG. Tracer arrival timing-insensitive technique for estimating flow in MR perfusion-weighted imaging using singular value decomposition with a block-circulant deconvolution matrix. Magn Reson Med 2003;50:164−174.

30. Press WA, Vetterling WT, Flannery BP, Teukolsky SA. Numerical recipes in C: the art of scientific computing. 2nd ed. Cambridge: Cambridge University Press; 1992. p 1−8.

31. Canny J. A computational approach to edge-detection. IEEE Trans Pattern Anal Machine Intell 1986;8:679−698.

32. Hrabe J, Lewis DP. Two analytical solutions for a model of pulsed arterial spin labeling with randomized blood arrival times. J Magn Reson 2004;167:49−55.

33. Leenders KL, Perani D, Lammertsma AA, Heather JD, Buckingham P, Healy MJ, Gibss JM, Wise RJ, Hatazawa J, Herold S, Beaney RP, Brooks DJ, Spinks T, Rhodes C, Frackowiak RS, Jones T. Cerebral blood flow, blood volume and oxygen utilization: normal values and effect of age. Brain 1990;113:27−47.

34. Calamante F, Gadian DG, Connelly A. Quantification of bolus-tracking MRI: improved characterization of the tissue residue function using Tikhonov regularization. Magn Reson Med 2003;50:1237−1247.

35. Calamante F, Gadian DG, Connelly A. Delay and dispersion effects in dynamic susceptibility contrast MRI: simulations using singular value decomposition. Magn Reson Med 2000;44:466−473.

36. Wu O, Ostergaard L, Koroshetz WJ, Schwamm LH, O'Donnell J, Schaefer PW, Rosen BR, Weisskoff RM, Sorensen AG. Effects of tracer arrival time on flow estimates in MR perfusion-weighted imaging. Magn Reson Med 2003;50:856−864.

37. Vonken EP, Beekman FJ, Bakker CJ, Viergever MA. Maximum likelihood estimation of cerebral blood flow in dynamic susceptibility contrast MRI. Magn Reson Med 1999;41:343−350.

38. An H, Lin W. Cerebral venous and arterial blood volumes can be estimated separately in humans using magnetic resonance imaging. Magn Reson Med 2002;48:583−588.

39. Greenberg JH, Alavi A, Reivich M, Kuhl D, Uzzell B. Local cerebral blood volume response to carbon dioxide in man. Circ Res 1978;43:324−331.

40. Silvennoinen MJ, Clingman CS, Golay X, Kauppinen RA, van Zijl PCM. Comparison of the dependence of blood R_2 and $R_2{}^*$ on oxygen saturation at 1.5 and 4.7 Tesla. Magn Reson Med 2003;49:47−60.